Advances in stable isotope tracer methodology part 1: hepatic metabolism via isotopomer analysis and postprandial lipolysis modeling

Cecilia Diniz Behn,[1,2] Eunsook S Jin,[3] Kate Bubar,[1] Craig Malloy,[3] Elizabeth J Parks,[4] Melanie Cree-Green [2,5]

[1]Applied Mathematics and Statistics, Colorado School of Mines, Golden, Colorado, USA
[2]Division of Endocrinology, Department of Pediatrics, University of Colorado Anschutz School of Medicine, Aurora, Colorado, USA
[3]Advanced Imaging Research Center, UT Southwestern Medical, Dallas, Texas, USA
[4]Department of Nutrition and Exercise Physiology, University of Missouri, Columbia, Missouri, USA
[5]Pediatric Endocrinology, Children's Hospital Colorado, Aurora, Colorado, USA

Correspondence to
Dr Melanie Cree-Green, University of Colorado Denver School of Medicine, Aurora, Colorado 80045-2581, USA; Melanie.Green@childrenscolorado.org

Accepted 10 July 2019
Published Online First 24 September 2019

► http://dx.doi.org/10.1136/jim-2019-001108

To cite: Diniz Behn C, Jin ES, Bubar K, *et al*. *J Investig Med* 2020;**68**:3–10.

ABSTRACT

Stable isotope tracers have been used to gain an understanding of integrative animal and human physiology. More commonly studied organ systems include hepatic glucose metabolism, lipolysis from adipose tissue, and whole body protein metabolism. Recent improvements in isotope methodology have included the use of novel physiologic methods/models and mathematical modeling of data during different physiologic states. Here we review some of the latest advancements in this field and highlight future research needs. First we discuss the use of an oral [U-$^{13}C_3$]-glycerol tracer to determine the relative contribution of glycerol carbons to hepatic glucose production after first cycling through the tricarboxylic acid cycle, entry of glycerol into the pentose phosphate pathway or direct conversion of glycerol into the glucose. Second, we describe an adaptation of the established oral minimal model used to define postprandial glucose dynamics to include glycerol dynamics in an oral glucose tolerance test with a [$^2H_5$]-glycerol tracer to determine dynamic changes in lipolysis. Simulation results were optimized when parameters describing glycerol flux were determined with a hybrid approach using both tracer-based calculations and constrained parameter optimization. Both of these methodologies can be used to expand our knowledge of not only human physiology, but also the effects of various nutritional strategies and medications on metabolism.

INTRODUCTION

Isotopes have been used to investigate physiology for over 80 years.[1] Many studies in humans use stable isotopes, which are not radioactive and are well-tolerated when used in physiologic concentrations.[2] General methods for the use of stable isotopes to study physiology and pathology have been well described[2 3] and the principal organs that drive overall whole-body metabolism include muscle, adipose, and the liver, with critical smaller roles played by the brain and skeletal system, among others.[2 3] Classic isotope assessments quantify the rate of appearance (Ra) of glucose from the liver, the rate of lipolysis from adipose tissue, measures of protein turnover and rates of the oxidation of glucose, fats and proteins/amino acids.[4 5] Continuous efforts have been employed to expand the types of physiologic pathways that can be measured and to improve the accuracy of existing models. Here, we describe two distinct advancements for the use of stable isotope tracers to assess human physiology.

Methods of sample analysis have traditionally involved the use of mass spectrometry to determine the isotopic enrichment of the compound of interest, paired with gas chromatography for better separation of compounds. Newer methods have replaced gas chromatography with high pressure liquid chromatography.[6] With mass spectrometry, selecting different methods of derivatization of the sample or different ion fragments for selective ion monitoring in the mass spectrometer supports the analysis of specific atoms within the fragment. Additional insights can be gained by combining tracers that interact through metabolic processes of interest, such as the tricarboxylic acid (TCA) cycle flux[7] or hepatic triglyceride synthesis[8] to name a few. More recently, nuclear magnetic resonance (NMR) has been used to more precisely quantitate isotopomers.[9] Herein we describe the application of this methodology combined with an oral glycerol tracer to assess relative hepatic pathway flux during the production of glucose.

Mathematical modeling of stable isotope data, such as the oral minimal model (OMM) used to describe glucose dynamics during an oral glucose tolerance test (OGTT),[10–12] can be critical for linking how the dynamics of a substrate are influenced by insulin sensitivity. Renewed interest has occurred in the study of adipocyte dysfunction, especially as it relates to rates of lipolysis, and glycerol dynamics provide insight into these processes. Here, we present an adaptation of the glucose-derived OMM that also uses glycerol to simultaneously measure postprandial lipolysis. Different methods for determining Ra glycerol were compared. One of the most widely applied techniques is the method originally proposed by Steele to describe dynamic changes in the Ra of a substrate when the organism (or cell) is in a physiologic steady state.[3 13] This approach was adapted for use in the non-steady state although applications of the non-steady state technique have not always

been successful.[14] Other model examples not discussed here include the use of mass isotopomer distribution analysis[15 16] for estimating an intracellular precursor enrichment when it cannot be measured and the use of data from a multi-step hyperinsulinemic-euglycemic clamp when basal Ra cannot be accurately assessed. In summary, we found that a hybrid approach using Steele's equation to calculate Ra at steady state, followed by use of constrained parameter estimation of Ra during the dynamic phase, minimized the error in simulated glycerol concentrations for both the fasting and dynamic portions of the curve.

Use of an oral glycerol drink combined with isotopomer analysis to understand hepatic metabolism

The liver plays a key role in metabolic homeostasis for the whole body. After a meal, the liver stores excess glucose as glycogen and can convert excess energy to triglycerides (TG) for export via very low-density lipoprotein particle secretion. Under fasting conditions, the liver produces glucose by either glycogenolysis or gluconeogenesis (GNG) from lactate, pyruvate, amino acids, or glycerol. Among these substrates, only glycerol is released from adipose tissues through the hydrolysis of TG, and it is readily used by the liver due to this organ's high level of the enzyme, glycerol kinase.[17] Further, unlike other GNG substrates, glycerol incorporation into newly-synthesized glucose does not require metabolism through the TCA cycle. Thus, when the liver is exposed to glycerol, phosphorylated glycerol (ie, glycerol 3-phosphate, G3P) can be converted to dihydroxyacetone phosphate (DHAP) or glyceraldehyde 3-phosphate (GA3P). These trioses are in rapid exchange via the enzyme triose phosphate isomerase, and their condensation leads to glucose synthesis. Labeling these GNG processes with [U-$^{13}C_3$]-glycerol produces a triple-labeled ([1,2,3-$^{13}C_3$] or [4,5,6-$^{13}C_3$]) glucose; [U-$^{13}C_3$]-DHAP+GA3P → [1,2,3-$^{13}C_3$]-glucose, and DHAP + [U-$^{13}C_3$]-GA3P → [4,5,6-$^{13}C_3$]-glucose (figure 1A,B).

Experimental results, however, demonstrate the presence of numerous double-labeled glucose isotopomers including ([1,2-$^{13}C_2$]-glucose, [2,3-$^{13}C_2$]-glucose, [4,5-$^{13}C_2$]-glucose and [5,6-$^{13}C_2$]-glucose). Glucose that is triple-labeled also occurs through [U-$^{13}C_3$]-glycerol moving through GNG—as evidenced by ^{13}C NMR of a glucose derivative (figure 1A). The singlets (S) in the spectrum of figure 1A mainly reflect natural ^{13}C abundance. However, four doublets were also detected: signals from [1,2-$^{13}C_2$]-glucose, [2,3-$^{13}C_2$]-glucose, [4,5-$^{13}C_2$]-glucose, and [5,6-$^{13}C_2$]-glucose can also arise because of [U-$^{13}C_3$]-glycerol metabolism through the TCA cycle prior to GNG (figure 1C). Instead of direct incorporation into glucose, some [U-$^{13}C_3$]-glycerol is directed to glycolysis producing [U-$^{13}C_3$]-pyruvate. Pyruvate enters the TCA cycle through carboxylation via pyruvate carboxylase or decarboxylation via pyruvate dehydrogenase. After entry, ^{13}C-labels are extensively scrambled in the TCA cycle which label all the intermediates of the cycle. Oxaloacetate, an intermediate of the TCA cycle, may exit the cycle via phosphoenolypyruvate (PEP) carboxykinase producing mainly double-labeled ([2,3-$^{13}C_2$]-PEP and [1,2-$^{13}C_2$])-PEP under these conditions.[18] Continuous GNG processes from these PEP isotopomers lead to double-labeled glucose isotopomers; [2,3-$^{13}C_2$]-PEP→ [1,2-$^{13}C_2$]-glucose or [5,6-$^{13}C_2$]-glucose, and [1,2-$^{13}C_2$]-PEP → [2,3-$^{13}C_2$]-glucose or [4,5-$^{13}C_2$]-glucose. Thus, the appearance of double-labeled glucose is evidence of [U-$^{13}C_3$]-glycerol metabolism through the TCA cycle. However, the metabolism through the TCA cycle does not explain why the signal from [1,2-$^{13}C_2$]-glucose is much stronger than that from [5,6-$^{13}C_2$]-glucose because both isotopomers originate from a common source, [2,3-$^{13}C_2$]PEP.

The difference between [1,2-$^{13}C_2$]-glucose and [5,6-$^{13}C_2$]-glucose can be explained by the potential for glycerol carbons to route through the pentose phosphate pathway (PPP) in liver after [U-$^{13}C_3$]glycerol administration (figure 1D). As noted, [U-$^{13}C_3$]-glycerol direct incorporation into GNG produces [1,2,3-$^{13}C_3$]-hexose and [4,5,6-$^{13}C_3$]-hexose. When [1,2,3-$^{13}C_3$]-glucose 6-phosphate and [4,5,6-$^{13}C_3$]-glucose 6-phosphate enter the PPP, carbon 1 is lost in the oxidative phase of the pathway becoming [1,2-$^{13}C_2$]-pentose and [3,4,5-$^{13}C_3$]-pentose, respectively. The carbons of pentose are rearranged through multiple reactions in the non-oxidative phase of the PPP, producing mainly [1,2-$^{13}C_2$]-fructose 6-phosphate and [4,5,6-$^{13}C_3$]-fructose 6-phosphate, respectively, and consequently [1,2-$^{13}C_2$]-glucose and [4,5,6-$^{13}C_3$]-glucose. Thus additional [1,2-$^{13}C_2$]-glucose is generated through the full cycle of the PPP, causing higher [1,2-$^{13}C_2$]-glucose concentration than [5,6-$^{13}C_2$]-glucose.[18]

The pathways described above result in ^{13}C-labeling patterns in glucose after [U-$^{13}C_3$]-glycerol administration and these data provide rich information about three critical biochemical processes in liver. First, the sum of all ^{13}C-labeled glucose isotopomers indicates GNG from glycerol. Second, double-labeled glucose isotopomers reflect [U-$^{13}C_3$]-glycerol metabolism through the TCA cycle, demonstrating mitochondrial biosynthetic functions. In this case, [5,6-$^{13}C_2$]-glucose is a convenient biomarker because the signal is stronger than other double-labeled isotopomers and its production is independent from the PPP activity. Third, the difference between [1,2-$^{13}C_2$]-glucose and [5,6-$^{13}C_2$]-glucose (precisely, [1,2-$^{13}C_2$]/[2,3-$^{13}C_2$] vs [5,6-$^{13}C_2$]/[4,5-$^{13}C_2$] in glucose) reflects hepatic PPP activity.[18]

In addition to quantitating glucose production pathways, [U-$^{13}C_3$]-glycerol administration can also label the backbone of TG (figure 2A). One necessary intermediate for fatty acid esterification producing TG is G3P, and the direct incorporation of [U-$^{13}C_3$]-glycerol into TG produces [U-$^{13}C_3$]-glycerol-TG (figure 2B). Similarly as noted above, the indirect incorporation into TG of glycerol that traversed the TCA cycle leads to double-labeled [1,2-$^{13}C_2$]-glycerol and [2,3-$^{13}C_2$]-glycerol backbones in TG (figure 2C). Figure 2A shows ^{13}C-NMR of glycerol backbones in TG from lipid extracts after infusion with [U-$^{13}C_3$]-glycerol. The doublet in the glycerol backbone C1 & C3 region is a signal from both double-labeled and triple-labeled glycerol reflecting overall ^{13}C enrichments in the backbones. In contrast, the doublet in the glycerol backbone C2 region is the signal from both [1,2-$^{13}C_2$]-glycerol and [2,3-$^{13}C_2$]-glycerol, while the triplet is the signal from [U-$^{13}C_3$]-glycerol only, reflecting [U-$^{13}C_3$]-glycerol's indirect incorporation through the TCA cycle and direct incorporation to TG, respectively.[19]

The [U-$^{13}C_3$]-glycerol method above was originally developed using rodent models, but has now been translated to clinical studies. In animal studies, after a [U-$^{13}C_3$]-glycerol

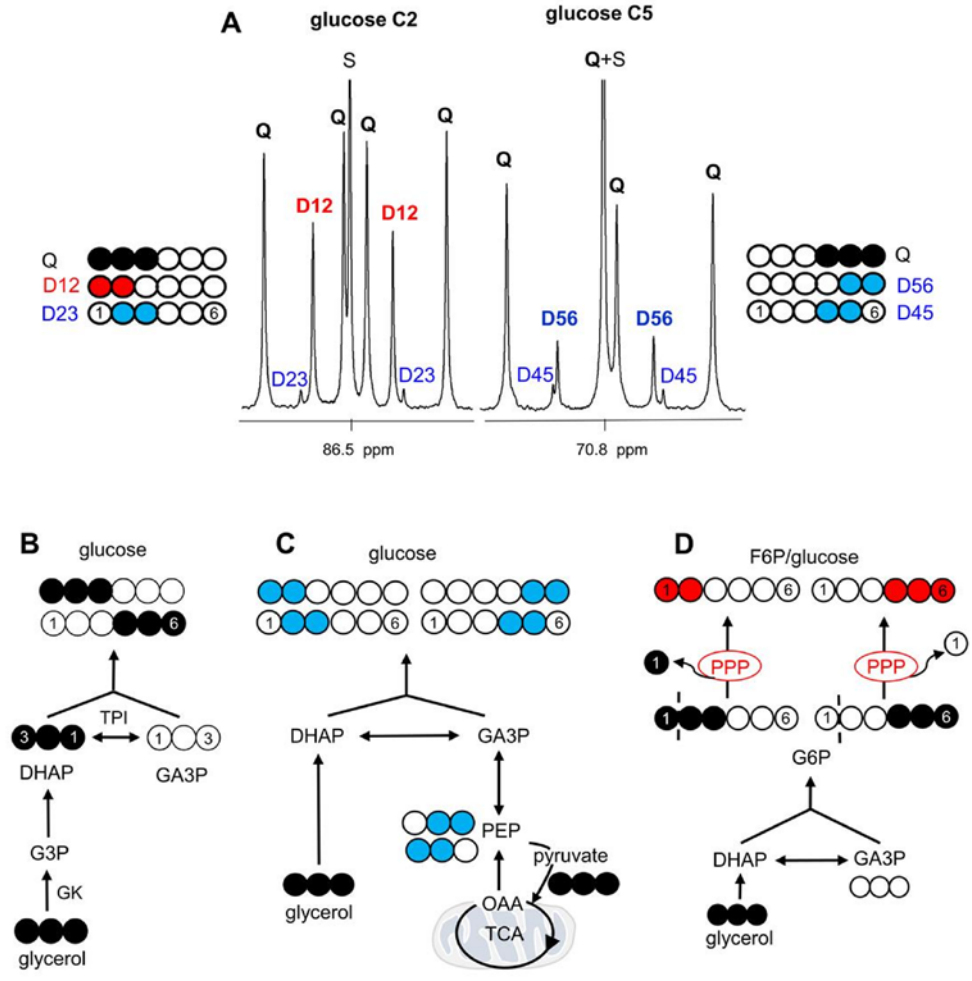

Figure 1 [U-$^{13}C_3$]-glycerol incorporation into glucose. (A)^{13}C NMR of glucose derivative shows signals from glucose isotopomers derived from blood of a rat receiving [U-$^{13}C_3$]-glycerol. (B) [U-$^{13}C_3$]-glycerol direct incorporation into glucose produces triple-labeled ([1,2,3-$^{13}C_3$]-glucose or [4,5,6-$^{13}C_3$])-glucose. (C) [U-$^{13}C_3$]-glycerol metabolism through the TCA cycle prior to gluconeogenesis produces double-labeled [1,2-$^{13}C_2$]-glucose, [2,3-$^{13}C_2$]-glucose, [4,5-$^{13}C_2$]-glucose or [5,6-$^{13}C_2$]-glucose. (D) If [1,2,3-$^{13}C_3$]-hexose and [4,5,6-$^{13}C_3$]-hexose enter the PPP, carbon 1 is lost in the oxidative phase followed by carbon rearrangement in the non-oxidative phase. Consequently [1,2-$^{13}C_2$]-hexose and [4,5,6-$^{13}C_3$]-hexose are produced from [1,2,3-$^{13}C_3$]-hexose and [4,5,6-$^{13}C_3$]-hexose, respectively, through the PPP. Open circle, ^{12}C; black circle, ^{13}C; blue circle, ^{13}C after movement through the TCA cycle; red circle, ^{13}C after experiencing the PPP. DHAP, dihydroxyacetone phosphate; F6P, fructose 6-phosphate; GA3P, glyceraldehyde 3-phosphate; GK, glycerol kinase; G3P, glycerol 3-phosphate; G6P, glucose 6-phosphate; NMR, nuclear magnetic resonance; OAA, oxaloacetate; PEP, phosphoenolpyruvate; PPP, pentose phosphate pathway, TCA, tricarboxylic acid; TPI, triose phosphate isomerase.

intraperitoneal injection (0.5 g/kg body weight), liver and blood were harvested for lipid and glucose extraction followed by ^{13}C NMR analysis. In clinical studies, liver tissue is not readily available, but blood samples can be used for analysis because TG and glucose synthesized in liver are released into the circulation. The study procedures in a clinical study are quite simple requiring research subjects to drink water containing [U-$^{13}C_3$]-glycerol and blood draws over a 3–6-hour period. The [U-$^{13}C_3$]-glycerol method has been applied in a few clinical studies as proof of concept.[9 20 21]

One published study examined hepatic metabolism in patients with fatty liver but without other clinical manifestations.[20] Obese, but otherwise healthy subjects were recruited and their intrahepatic TG were measured using proton magnetic resonance spectroscopy. All volunteers received ^2H_2O (5 g/kg body water—calculated as 60% of body weight for men or 50% of body weight for women)[20–22] and 50 mg/kg body weight [U-$^{13}C_3$]-glycerol orally, after an overnight fast, followed by a series of blood draws up to 240 minutes after the glycerol administration. Blood samples were processed for NMR analysis of TG and glucose as described.[9]^{13}C NMR analysis of TG-glycerol demonstrated that patients with hepatic steatosis (>5% fats) had lower ^{13}C enrichments in the glycerol backbones compared with controls (≤5% fats), supporting TG-[^{13}C]-glycerol dilution by a larger TG pool or greater unlabeled glycerol flux. The subjects also exhibited faster and greater [U-$^{13}C_3$]-glycerol

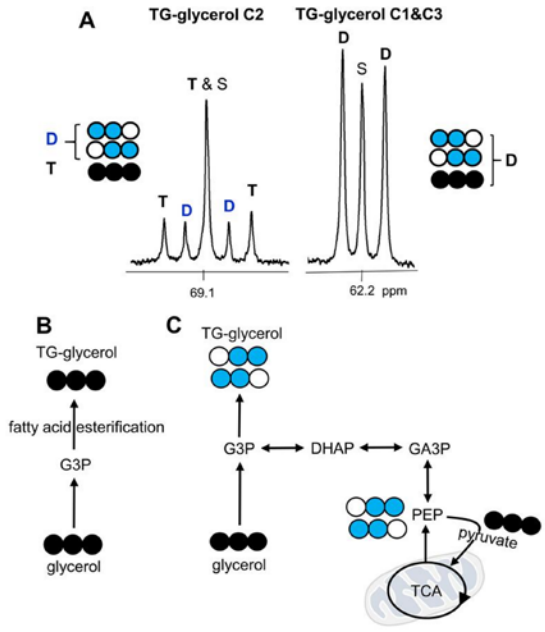

Figure 2 [U-$^{13}C_3$]-glycerol incorporation into triglycerides. (A)^{13}C NMR of lipid extracts shows signals from glycerol backbones of TG derived from blood of a subject receiving [U-$^{13}C_3$]-glycerol. (B) [U-$^{13}C_3$]-glycerol direct incorporation into TG produces triple-labeled glycerol backbones. (C) [U-$^{13}C_3$]-glycerol indirect contribution to TG through the TCA cycle produces double-labeled glycerol backbones. Open circle, ^{12}C; black circle, ^{13}C; blue circle, ^{13}C after experiencing the TCA cycle. DHAP, dihydroxyacetone phosphate; GA3P, glyceraldehyde 3-phosphate; G3P, glycerol 3-phosphate; NMR, nuclear magnetic resonance; PEP, phosphoenolpyruvate; TG, triglycerides; TCA, tricarboxylic acid.

metabolism through the TCA cycle prior to TG incorporation than controls. ^{13}C NMR analysis of plasma glucose demonstrated delayed GNG from [U-$^{13}C_3$]-glycerol in those with fatty liver, while ^{2}H NMR analysis of glucose demonstrated that the relative contributions to glucose production from glycogen, glycerol and the TCA cycle were similar between those with and without fatty liver. However, after the oral glycerol load, compared with the control subjects, those with fatty liver demonstrated slower changes in fluxes contributing to hepatic glucose production. The load of [U-$^{13}C_3$]-glycerol led to a transient increase of the glycerol contribution to glucose, and this was in concordance with decreased glycogen contribution in all participants.

This method has been tested during the fasted state, as described above, following a meal and more recently, following an OGTT.[9 22 23] The timing for the glycerol drink and optimal timing of the sample collection varies per type of oral challenge, as well as with the type of patient population. During the OGTT, the timing of the serum sampling needs to occur after peak suppression of Ra glucose when hepatic glucose release is starting to return to fasted rates, to ensure that enrichments are high enough for detection. This will occur at a later timepoint in populations with lower insulin sensitivity and will also be delay even more so after meals.[23]

In summary, NMR analysis combined with [U-$^{13}C_3$]-glycerol and $^{2}H_2O$ stable isotopes is a very convenient method, suitable for outpatients, that enables investigation of multiple hepatic biochemical processes in human subjects with only blood sampling from a single intravenous access site and an oral tracer.

Modeling changes in lipolysis following a glucose challenge

During lipolysis, breakdown of adipose tissue releases glycerol and non-esterified fatty acids (NEFA) for use as an energy substrates. Insulin resistance (IR) at the level of the adipose tissue is characterized by slow or incomplete suppression of lipolysis in response to insulin, and this may contribute to the development or progression of IR in other tissues.[24] Therefore, improved understanding of adipose IR is imperative for advancing the care and treatment of diabetes and other metabolic disorders, particularly in populations such as obese adolescents, with rapid disease progression and high disease severity.[25 26]

Although disorders of lipolysis typically manifest in the postprandial state, most measures of adipose IR, including the gold standard multi-phase hyperinsulinemic-euglycemic clamp, focus on NEFA, glycerol and insulin concentrations under fasted or other steady-state conditions.[27–30] Furthermore, combining a glycerol tracer with a clamp allows for the assessment of Ra glycerol, a direct marker of lipolysis which is less affected by intracellular recycling and the direct effect of insulin on uptake compared with NEFA.[24–26 31–33] Experimental protocols such as the OGTT offer a more physiologic setting for assessing insulin sensitivity. However, interpretation of dynamic OGTT data, such as time-varying glucose, insulin, glycerol and NEFA concentrations, can be complex, and measures that have attempted to include OGTT data in assessments of adipose IR may be unreliable in subjects with pancreatic β-cell dysfunction.[28]

Mathematical models have been developed based on glucose concentrations during an OGTT using data with[10] and without[11 34] glucose tracers. These models have provided insight into the connections between glucose dynamics and whole-body, and hepatic-specific, insulin sensitivity. In addition, models focusing on the dynamics of NEFA have been proposed, although, to our knowledge, this approach has not been used to describe OGTT glycerol dynamics.[29 35 36] To address this gap, we developed a novel, one-compartment, differential equation-based mathematical model to describe plasma glycerol dynamics during an OGTT with a glycerol isotope tracer. Ra glycerol is a key component of the model, and different approaches may be used to calculate or estimate this quantity.[10 32 37] We compared these methodologies to determine the optimal implementation of Ra to include in the model to describe lipolysis and produce accurate representations of simulated glycerol concentrations.

METHODS

Subjects: Fifteen participants, ages 12 to 21, were recruited from pediatric clinics at the Children's Hospital Colorado for a prospective, cross-sectional study. The participants were overweight/obese girls (body mass index ≥ 90thpercentile for age). All participants were sedentary and had

achieved Tanner Stage 5 in puberty. Exclusion criteria included type 2 diabetes and medications that affect insulin sensitivity. Data were collected as part of the cross-sectional trial APPLE (liver and fat regulation in overweight adolescent girls; NCT02157974) and all participants provided assent or consent (≥18 years of age) with consent from the guardian in children.

Study protocol: One day prior to admission, participants consumed an isocaloric diet (55% carbohydrate, 15% protein, 30% fat) and refrained from physical activity. Following an overnight fast, the participants underwent a primed constant intravenous infusion of [$^2H_5$]-glycerol starting at 06:00 AM. Baseline blood samples were obtained. At 08:00 AM, an OGTT with 75 g glucose was initiated, and blood was frequently sampled over 4 hours at times t=−30,–20, −10, 0, 10, 20, 30, 45, 60, 75, 90, 105, 120, 135, 150, 180, 210, and 240. Analysis of [$^2H_5$]-glycerol was performed using gas chromatography mass spectrometry as previously described.[25 26 31 37] All isotopic measurements were corrected for background enrichment.

Mathematical model of glycerol: To describe glycerol dynamics in plasma, we developed a one-compartment model in which the change in glycerol concentration is given by the following equation:

$$\frac{dg(t)}{dt} = -S_g g(t) + \frac{Ra(t)}{V}$$

where $g(t)$ represents glycerol concentration; $Ra(t)$ is the rate of appearance of glycerol; and parameters S_g and V represent the glycerol clearance rate and volume of distribution, respectively.

Ra(t) is approximated by a piecewise linear function:

$$\mathrm{Ra}(t) = \begin{cases} \alpha_{i-1} + \frac{\alpha_i - \alpha_{i-1}}{t_i - t_{i-1}}\left(t - t_{i-1}\right), & t_{i-1} \le t \le t_i \\ 0, \textit{otherwise} \end{cases}$$

for $i = 1, \ldots n$. Note that the action of insulin to suppress glycerol release is implicit in the representation of Ra(t). The breakpoints for the Ra(t) function are described below.

Fixing V=0.3 dL/kg to represent the glycerol pool by the estimated volume of plasma,[3] the model is structurally identifiable. The model is solved numerically using the MATLAB built-in solver ode45. Model parameters are estimated with a constrained optimization to fit glycerol concentrations using the MATLAB built-in function fmincon. A constrained optimization is performed to ensure that all estimated parameter values are non-negative.

Computing Ra: Three approaches were tested to determining the dynamic Ra glycerol represented by the α_i parameters in Ra(t): calculating α_i using Steele's non-steady state equation adapted for use with stable isotopes (Steele's Ra)[3 32]; estimating Ra(t) with $\alpha_i \ge 0$ for all i (estimated Ra); and estimating Ra(t) with the constraints that α_0=calculated Steele's α_0 and $\alpha_i \ge 0$ for all i (constrained Ra). For Steele's Ra, the α_i was calculated at each sampling time point to minimize error associated with large changes in enrichment over time. For estimated and constrained Ra, the α_i were estimated at a subset of those time points (t=0, 10, 30, 60, 90, 120, 180, and 240) to balance model flexibility with the number of parameters to be estimated from the data as has previously been described for approximating Ra glucose.[10]

Comparing Ra and simulation results: We expected α_0 to give a measure of lipolysis in the fasted state analogous to the baseline stage of the hyperinsulinemic-euglycemic clamp.[25 26 38 39] To compare the estimates of α_0 resulting from different methods, we used box and whisker plots and applied the Wilcoxon signed-rank test to values of α_0 paired by participant. We also used Bland-Altman plots to compare estimates of α_0, and we report the bias ±95% CIs and limits of agreement for the Bland-Altman plots.

Each representation of Ra produced a simulated time trace of glycerol concentration during the OGTT. To compare the performance of each representation of Ra, we computed the least-squares error between simulated glycerol time traces and measured glycerol data. We compared the errors associated with each method using box and whisker plots and the Wilcoxon signed-rank test on errors paired by participant.

RESULTS

Ra glycerol varied depending on different methods. As described above, we determined the parameters α_i in the representation of Ra glycerol using several different methods denoted as Steele's Ra, estimated Ra, and constrained Ra. These methods produced different profiles for Ra(t) (figure 3). All profiles exhibited a reduction of Ra glycerol following the glucose drink. However, the estimate of Ra at baseline given by α_0 was higher for Steele's Ra compared with estimated Ra (median 3.44 for Steele's Ra and 1.09 for estimated Ra; p=3.05e-04; figure 3B). Bland-Altman plots showed that the α_0 associated with estimated Ra had a bias of −1.99 with 95% CI of the bias (−2.7457 to −1.2355) compared with Steele's Ra. The 95% limits of agreement were (−4.6631 to 0.6818), although interpretation of these values was limited by the small sample size. Steele's Ra was generally larger than estimated Ra across the OGTT except in subjects for whom the recovery of Steele's Ra values lagged behind the recovery of glycerol concentrations in a non-physiologic way. Estimated and constrained Ra values recovered in conjunction with recovery of glycerol concentrations in all participants.

Simulated glycerol sensitive to Ra. Across the OGTT, glycerol concentrations fell in response to increased insulin concentrations in all participants (figure 4). The simulated glycerol concentrations were sensitive to the representation of Ra, however, for all Ra the simulated glycerol profiles showed the stereotypical reduction associated with suppression of lipolysis during an OGTT. For each method, we computed the least-squares error between the simulated glycerol concentrations and the measured glycerol concentrations across the OGTT. We found that the error between these concentrations was greatest for Steele's Ra compared with the estimated or constrained Ra (both p=6.103e-05). The error associated with the constrained Ra was higher compared with the estimated Ra (p=0.001), but the median values were close (23.42 for constrained Ra; 18.45 for estimated Ra) compared with the median value for Steele's Ra (82.40) (figure 4B). Model simulations using the constrained Ra successfully described glycerol data in reflecting different glycerol and insulin profiles (figure 4C-H).

We found that the one-compartment-based mathematical model robustly described the suppression and recovery of glycerol concentrations during an OGTT for youth with different patterns of glycerol and insulin concentrations.

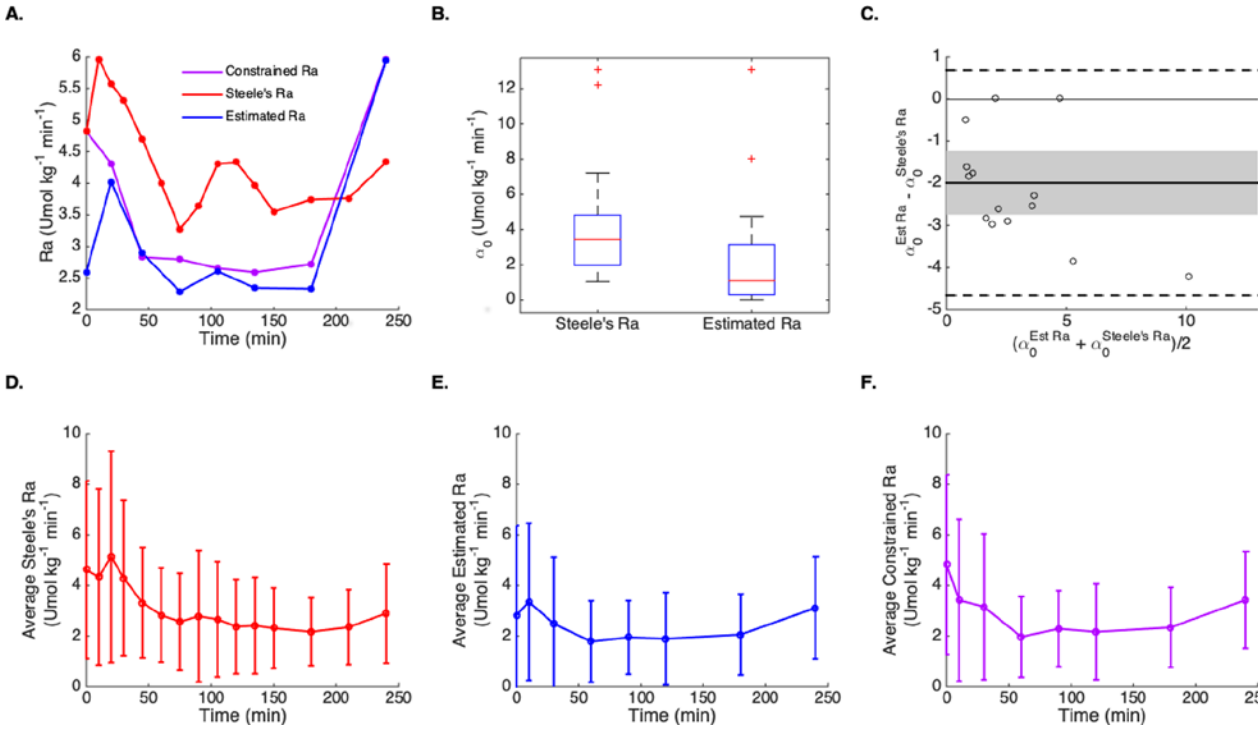

Figure 3 Comparison of Steele's calculation, and estimated and constrained models to calculate glycerol Ra. The Ra of glycerol is a key output of the mathematical model of glycerol dynamics. (A) Computing (Steele's Ra) or estimating (estimated and constrained Ra) the Ra-glycerol for a representative research subject produces different characterizations of lipolysis across the OGTT. (B) The parameter α_0 represents Ra-glycerol at baseline (time t=0), and α_0 calculated with Steele's non-steady state equation is greater compared with α_0 estimated from the glycerol data (Wilcoxon signed-rank test, *P*=0.0003). (C) Bland-Altman plots show that the α_0 in estimated Ra is lower than α_0 in Steele's Ra with a bias of −1.99±0.76 (95% CI). (D–F) Representations of average Ra across subjects demonstrated different profiles for Steele's Ra (D), Estimated Ra (E), and Constrained Ra (F). OGTT, oral glucose tolerance test; Ra, rate of appearance.

Simulated glycerol time traces depended on the representation of Ra glycerol, and data were better fit by simulations using estimated and constrained Ra compared with Steele's Ra.

The improved fit to glycerol data produced by estimated Ra compared with Steele's Ra was likely caused, in part, by simulated glycerol traces for individuals for whom Steele's Ra failed to recover in conjunction with measured glycerol concentrations. The delayed recovery of Steele's Ra for some participants suggests that additional factors, such as recycling of the glycerol tracer, may affect measured enrichments.[3] Similarly, other well-described sources of error in Steele's non-steady state equation applied to calculate Ra glucose likely also apply to Ra glycerol. These include a variable volume of distribution; sensitivity to the change in enrichment (particularly when enrichment is changing quickly), and potential multi-exponential washout kinetics.[3] However, glycerol uptake is typically proportional to glycerol concentration over physiological ranges.[40] For example, Steele's Ra is unable to compensate for time-dependent changes in the volume of distribution, but these changes may be absorbed in the parameters representing estimated Ra. This contributes to a poorer fit of simulated glycerol concentrations compared with measured glycerol concentrations when Steele's Ra is used in the model.

By contrast, non-steady state errors should not affect Steele's Ra at baseline when enrichment, distribution volume, and uptake are essentially constant analogous to its application in the clamp.[24–26 31 32] Therefore, the systematic difference between estimated Ra and Steele's Ra at baseline suggests that estimated Ra may not accurately reflect lipolysis rates across the OGTT. The constrained Ra combines the features of Steele's Ra and estimated Ra by constraining Ra to be equal to Steele's Ra at baseline (α_0) and allowing the other α_i parameters to be estimated based on measured glycerol concentrations. Thus, the constrained Ra describes a glycerol appearance rate that reflects lipolysis at baseline and, when implemented in the model, produces simulated glycerol concentrations that are consistent with measured glycerol concentrations across the OGTT for participants with different glycerol and insulin profiles. Future work is needed to validate the constrained Ra as a predictor of lipolysis in the dynamic setting of the OGTT and explore mathematical modeling frameworks that incorporate additional physiological complexity of insulin-mediated suppression of lipolysis.

CONCLUSIONS

Stable isotope tracer methodologies represent an important tool to advance the understanding of physiology within in the whole body and also in individual organs. In this article, we have described (1) a methodological advance for the study of hepatic metabolism and (2) a model adaptation for a postprandial measure of lipolysis. When combined with an oral glycerol tracer, isotopomer analysis can be used to

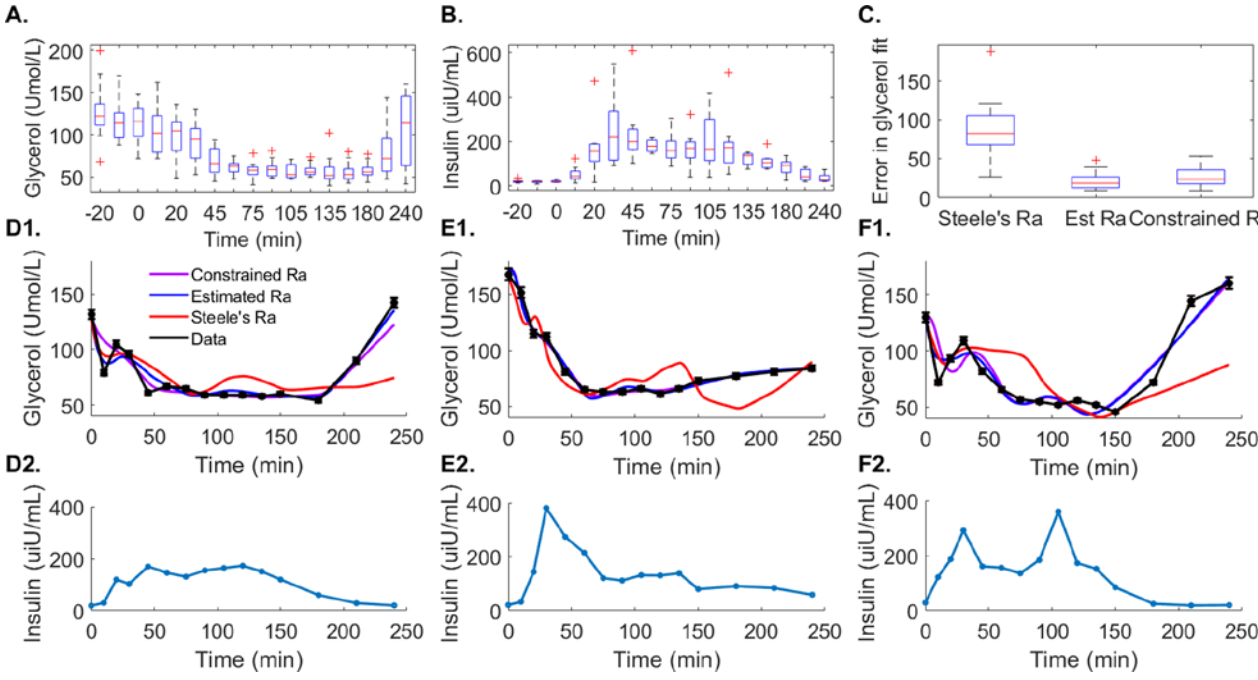

Figure 4 Calculated glycerol concentrations using Steele's calculation, and estimated and constrained models in participants with varying degrees of insulin resistance . Changes in serum glycerol and insulin concentrations during the OGTT and the dependence of simulated glycerol concentrations on the representation of Ra-glycerol. (A,B) Serum glycerol concentrations fall during the OGTT (A) in response to increases in insulin (B). (C) The error between simulated and measured glycerol concentrations is greatest when glycerol is simulated using Steele's Ra (median 82.40) compared with Estimated Ra (median 18.45) or Constrained Ra (median 23.42); Wilcoxon signed-rank test, (both p=6.103e-05). (D1,2)–(F1,2) Glycerol and simulated glycerol (D1, E1, F1) concentrations and insulin concentrations (D2, E2, F2) for three representative subjects with different glycerol-insulin profiles. The goodness-of-fit of the simulated glycerol concentrations varied with the implementation of different Ra-glycerol calculations. OGTT, oral glucose tolerance test; Ra, rate of appearance.

quantitate the movement of carbons down glycolysis and through the hepatic TCA or up toward the PPP. These alternate fates of glycerol were compared with its contribution more directly to the production of glucose through GNG. The initial OGTT glycerol model using Steele's calculation resulted in an estimated Ra that did not accurately describe glycerol concentrations in the post-OGTT state. Rather, representation of Ra using Steele's equation to calculate basal Ra and estimating the remainder of the Ra parameters using glycerol data offered the best solution. The continued method development in the field of isotope tracers is both necessary and exciting for the advancement of our understanding of how physiology is altered during feeding and in states of insulin resistance.

Acknowledgements The authors would like to thank the research participants for their time.

Contributors CDB, JE and MC-G researched the data wrote the manuscript. KB, CM, EJP researched the data and edited the manuscript.

Funding JE: NIH DK099289; CM: NIH National Institute of Biomedical Imaging and Bioengineering (NIBIB) P41 EB015908; MC-G: NIH BIRCWH K12HD057022, NIH K23DK107871, Children's Hospital Colorado, Doris Duke Foundation FCRS 2015212; NIH/NCATS Colorado CTSA Grant Number UL1 TR002535. The contents are the authors' sole responsibility and do not necessarily represent official NIH views.

Disclaimer MC-G has received product from AminoCorp, LLC.

Competing interests Yes, there are competing interests for one or more authors and I have provided a Competing Interests statement in my manuscript.

Patient consent for publication Not requred.

Provenance and peer review Not commissioned; internally peer reviewed.

ORCID iD
Melanie Cree-Green http://orcid.org/0000-0003-1593-1695

REFERENCES

1 Wilkinson DJ. Historical and contemporary stable isotope tracer approaches to studying mammalian protein metabolism. *Mass Spectrom Rev* 2018;37:57–80.
2 Kim IY, Suh SH, Lee IK, *et al*. Applications of stable, nonradioactive isotope tracers in in vivo human metabolic research. *Exp Mol Med* 2016;48:e203.
3 Wolfe RR, Chinkes DL. *Isotope Tracers in Metabolic Research. Principles and Practice of Kinetic Analysis*. Hoboken, NJ: Wiley-Liss, 2005.
4 Schellekens RC, Stellaard F, Woerdenbag HJ, *et al*. Applications of stable isotopes in clinical pharmacology. *Br J Clin Pharmacol* 2011;72:879–97.
5 Parks EJ, Matthews DE. A.S.P.E.N. 2003 Research Workshop on using tracers to measure carbohydrate, fat, and amino acid metabolism in humans. *JPEN J Parenter Enteral Nutr* 20042004;28:38–53.
6 Sun D, Cree MG, Zhang XJ, *et al*. Measurement of stable isotopic enrichment and concentration of long-chain fatty acyl-carnitines in tissue by HPLC-MS. *J Lipid Res* 2006;47:431–9.
7 Sunny NE, Parks EJ, Browning JD, *et al*. Excessive hepatic mitochondrial TCA cycle and gluconeogenesis in humans with nonalcoholic fatty liver disease. *Cell Metab* 2011;14:804–10.
8 Lambert JE, Ramos-Roman MA, Browning JD, *et al*. Increased de novo lipogenesis is a distinct characteristic of individuals with nonalcoholic fatty liver disease. *Gastroenterology* 2014;146:726–35.
9 Jin ES, Sherry AD, Malloy CR. An Oral Load of [13C3]Glycerol and Blood NMR Analysis detect fatty acid esterification, pentose phosphate pathway, and glycerol metabolism through the tricarboxylic acid cycle in human liver. *J Biol Chem* 2016;291:19031–41.
10 Dalla Man C, Caumo A, Cobelli C. The oral glucose minimal model: estimation of insulin sensitivity from a meal test. *IEEE Trans Biomed Eng* 2002;49:419–29.

11 Dalla Man C, Yarasheski KE, Caumo A, *et al*. Insulin sensitivity by oral glucose minimal models: validation against clamp. *Am J Physiol Endocrinol Metab* 2005;289:E954–E959.
12 Pyle L, Bergman BC, Nadeau KJ, *et al*. Modeling changes in glucose and glycerol rates of appearance when true basal rates of appearance cannot be readily determined. *Am J Physiol Endocrinol Metab* 2016;310:E323–E331.
13 Steele R. Influences of glucose loading and of injected insulin on hepatic glucose output. *Ann N Y Acad Sci* 1959;82:420–30.
14 Reeds PJ, Hachey DL, Patterson BW, *et al*. VLDL apolipoprotein B-100, a potential indicator of the isotopic labeling of the hepatic protein synthetic precursor pool in humans: studies with multiple stable isotopically labeled amino acids. *J Nutr* 1992;122:457–66.
15 Hellerstein MK, Neese RA. Mass isotopomer distribution analysis: a technique for measuring biosynthesis and turnover of polymers. *Am J Physiol* 1992;263(5 Pt 1):E988–1001.
16 Parks EJ, Hellerstein MK. Carbohydrate-induced hypertriacylglycerolemia: historical perspective and review of biological mechanisms. *Am J Clin Nutr* 2000;71:412–33.
17 Lin EC. Glycerol utilization and its regulation in mammals. *Annu Rev Biochem* 1977;46:765–95.
18 Jin ES, Sherry AD, Malloy CR. Interaction between the pentose phosphate pathway and gluconeogenesis from glycerol in the liver. *J Biol Chem* 2014;289:32593–603.
19 Jin ES, Sherry AD, Malloy CR. Metabolism of glycerol, glucose, and lactate in the citric acid cycle prior to incorporation into hepatic acylglycerols. *J Biol Chem* 2013;288:14488–96.
20 Jin ES, Browning JD, Murphy RE, *et al*. Fatty liver disrupts glycerol metabolism in gluconeogenic and lipogenic pathways in humans. *J Lipid Res* 2018;59:1685–94.
21 Landau BR, Wahren J, Chandramouli V, *et al*. Use of 2H2O for estimating rates of gluconeogenesis. Application to the fasted state. *J Clin Invest* 1995;95:172–8.
22 Jones JG, Solomon MA, Cole SM, *et al*. An integrated (2)H and (13)C NMR study of gluconeogenesis and TCA cycle flux in humans. *Am J Physiol Endocrinol Metab* 2001;281:E848–56.
23 Carreau AM, Jin ES, Garcia-Reyes Y, *et al*. A simple method to monitor hepatic gluconeogenesis and triglyceride synthesis following oral sugar tolerance test in obese adolescents. *Am J Physiol Regul Integr Comp Physiol* 2019;317:R134–R142.
24 Magkos F, Fabbrini E, Conte C, *et al*. Relationship between adipose tissue lipolytic activity and skeletal muscle insulin resistance in nondiabetic women. *J Clin Endocrinol Metab* 2012;97:E1219–E1223.
25 Cree-Green M, Bergman BC, Coe GV, *et al*. Hepatic Steatosis is Common in Adolescents with Obesity and PCOS and Relates to De Novo Lipogenesis but not Insulin Resistance. *Obesity* 2016;24–2399–406.
26 Cree-Green M, Wiromrat P, Stuppy JJ, *et al*. Youth with type 2 diabetes have hepatic, peripheral, and adipose insulin resistance. *Am J Physiol Endocrinol Metab* 2019;316:E186–E195.
27 Grenier-Larouche T, Carreau AM, Geloën A, *et al*. Fatty Acid Metabolic Remodeling During Type 2 Diabetes Remission After Bariatric Surgery. *Diabetes* 2017;66:2743–55.
28 Gastaldelli A, Gaggini M, DeFronzo RA. Role of Adipose Tissue Insulin Resistance in the Natural History of Type 2 Diabetes: Results From the San Antonio Metabolism Study. *Diabetes* 2017;66:815–22.
29 Søndergaard E, Espinosa De Ycaza AE, Morgan-Bathke M, *et al*. How to Measure Adipose Tissue Insulin Sensitivity. *J Clin Endocrinol Metab* 2017;102:1193–9.
30 Søndergaard E, Jensen MD. Quantification of adipose tissue insulin sensitivity. *J Investig Med* 2016;64:989–91.
31 Cree-Green M, Bergman BC, Cengiz E, *et al*. Metformin Improves Peripheral Insulin Sensitivity in Youth With Type 1 Diabetes. *J Clin Endocrinol Metab* 2019;104:3265–78.
32 Coppack SW, Persson M, Judd RL, *et al*. Glycerol and nonesterified fatty acid metabolism in human muscle and adipose tissue in vivo. *Am J Physiol* 1999;276:E233–E240.
33 Ramos-Roman MA, Lapidot SA, Phair RD, *et al*. Insulin activation of plasma nonesterified fatty acid uptake in metabolic syndrome. *Arterioscler Thromb Vasc Biol* 2012;32:1799–808.
34 Basu R, Di Camillo B, Toffolo G, *et al*. Use of a novel triple-tracer approach to assess postprandial glucose metabolism. *Am J Physiol Endocrinol Metab* 2003;284:E55–E69.
35 Periwal V, Chow CC, Bergman RN, *et al*. Evaluation of quantitative models of the effect of insulin on lipolysis and glucose disposal. *Am J Physiol Regul Integr Comp Physiol* 2008;295:R1089–R1096.
36 Boston RC, Moate PJ. NEFA minimal model parameters estimated from the oral glucose tolerance test and the meal tolerance test. *Am J Physiol Regul Integr Comp Physiol* 2008;295:R395–R403.
37 Bergman BC, Howard D, Schauer IE, *et al*. Features of hepatic and skeletal muscle insulin resistance unique to type 1 diabetes. *J Clin Endocrinol Metab* 2012;97:1663–72.
38 Jensen MD, Chandramouli V, Schumann WC, *et al*. Sources of blood glycerol during fasting. *Am J Physiol Endocrinol Metab* 2001;281:E998–E1004.
39 Jensen MD, Ekberg K, Landau BR. Lipid metabolism during fasting. *Am J Physiol Endocrinol Metab* 2001;281:E789–E793.
40 Winkler B, Steele R, Altszuler N. Effects of growth hormone administration on free fatty acid and glycerol turnover in the normal dog. *Endocrinology* 1969;85:25–30.